Electrochimica Acta 148 (2014) 266–275

Contents lists available at ScienceDirect

Electrochimica Acta

journal homepage: www.elsevier.com/locate/electacta

Electrochemical and Spectroelectrochemical Study of A_4 and A_2B_2 Pyrene Dendronized Porphyrins

Elizabeth K. Galván-Miranda [a], Gerardo Zaragoza-Galán [b,1], Ernesto Rivera [b], Martha Aguilar-Martínez [a], Norma A. Macías-Ruvalcaba [a,*]

[a] Facultad de Química, Universidad Nacional Autónoma de México, Ciudad Universitaria, C.P. 04510 México D.F., México
[b] Instituto de Investigaciones en Materiales, Universidad Nacional Autónoma de México, Ciudad Universitaria, C.P. 04510 México D.F., México

ARTICLE INFO

Article history:
Received 21 August 2014
Received in revised form 9 October 2014
Accepted 10 October 2014
Available online 17 October 2014

Keywords:
porphyrin
dendrimer
spectroelectrochemistry
aprotic solvent
oxidation mechanism

ABSTRACT

The electrochemical behaviour of two free-base pyrene dendronized porphyrins, Por-$(Py_2G1)_2$, Por-$(Py_2G1)_4$, and their zinc metallated forms, Zn-Por-$(Py_2G1)_2$ and Zn-Por-$(Py_2G1)_4$, has been studied by cyclic voltammetry in CH_2Cl_2. The investigated compounds exhibit several oxidation processes. The study of five model molecules, equivalent to the nuclei and branches of the dendrimer, allowed the assignment of the different oxidation processes. The first oxidation, centered on the porphyrin ring, was also studied by in situ UV-vis spectroelectrochemistry in CH_2Cl_2 and THF for all the dendrimers. The electrooxidation in the thin layer spectroelectrochemical cell of the two free-base dendritic molecules shows spectral changes that suggest the formation of porphyrin diprotonated species, both in THF and CH_2Cl_2. Even though the electrochemical and spectroscopic characteristics of the solutions after exhaustive electrolysis in THF were consistent with the formation of these protonated species; in CH_2Cl_2, a paramagnetic species was obtained, and no further evidence of the formation of diprotonated species could be found. Two-electrons per molecule were consumed during the electrolysis in THF and only one-electron in CH_2Cl_2, the starting porphyrin was not regenerated by counterelectrolysis in any case. It was demonstrated that irradiation of the porphyrin itself accounts for the observed evolution of the UV–vis spectra in CH_2Cl_2. For the Zn dendronized porphyrins, the oxidation was a clean one-electron transfer, giving rise to the radical cation, subsequent reductive electrolysis regenerates the initial product.

1. Introduction

Because of the broad range of potential applications of dendrimers and hyperbranched polymers, the interest on these supramolecular structures has been increasing at an amazing rate [1–3]. Their applications expand to areas including sensors, medicine, electrochromic and electroluminescent devices, light harvesting, redox mediators and molecular electronics [4–6]. Dendrimers can be functionalized with multiple photoactive or electroactive units at the core, at the periphery, or throughout their entire structure. The proximity of these groups within the dendrimer structure results in interesting systems with the ability to form excimers and exciplexes; and also participate in Fluorescence Resonance Energy Transfer (FRET), and Charge Transfer (CT) processes [7]. The study of dendritic structures functionalized with energy and/or electron donor-acceptor groups provides insight into the fundamental processes occurring in such complex systems and on their future applications [8–11].

Recently, our research group reported the synthesis, characterization, and optical properties of a novel series of dendritic compounds containing a single porphyrin at the core and a varying number, two to eight, of pyrene units at the periphery. It was demonstrated that pyrene and porphyrin constitute an excellent donor-acceptor pair for FRET. Spectroscopic data showed that FRET efficiency was not affected by the number of pyrene units; but an increasing number of pyrene units led to a more efficient light collection [12]. On this basis, we believe that these compounds, combined with adequate electron acceptors such as carbon nanotubes or graphene, could function as electron donor elements for the preparation of new supramolecular assemblies, which can be used in artificial photosynthetic devices [13–17]. The pyrene units would function not only as anchor groups to the nanocarbon

* Corresponding author. Tel.: +52 5556223758.
E-mail addresses: e.galvan@comunidad.unam.mx (E.K. Galván-Miranda), ger210582@yahoo.com.mx (G. Zaragoza-Galán), riverage@unam.mx (E. Rivera), maguilarm07@gmail.com (M. Aguilar-Martínez), nmaciasr@unam.mx (N.A. Macías-Ruvalcaba).
[1] Present address: Facultad de Ciencias Químicas, Universidad Autónoma de Chihuahua, Campus Universitario 2, Apartado Postal 669, Chihuahua 31125, México.

http://dx.doi.org/10.1016/j.electacta.2014.10.038
0013-4686/

structure [15,18], but also as light harvesting units to funnel this energy towards the porphyrin center to induce the electron transfer to the carbon nanotube, mimicking natural photosynthesis [19]. It has been demonstrated that photoexcitation of assemblies consisting of porphyrin and nanocarbon structures produces an ultrafast charge separation that triggers the oxidation of the electron-donating porphyrin [11,14,15]. The removal of one-electron from the porphyrin core would lead to the formation of the π-radical cation, a key intermediate in charge transfer reactions involving porphyrins and metalloporphyrins.

The role of phorphyrins and metalloporphyrins as electron donors in artificial photosynthetic devices makes it necessary to deepen the understanding of the properties and stability of their radical cations. Electrochemical techniques are efficient tools for the generation, detection, and characterization of radical ions. The electrochemistry of free-base and metallated porphyrins has been extensively studied; on their voltammograms, these compounds display two one-electron reversible oxidation processes corresponding to the formation of the radical cation and the dication, respectively; and two one-electron reduction processes forming the radical anion and the dianion [20,21]. This behaviour suggests that, on the timescale of cyclic voltammetry, the radical cation of both types of porphyrins is stable. However, previous research on the chemical or electrochemical oxidation at larger timescales, points out that the chemical fate of the radical cations of the free-base porphyrins is different from that of the metallated ones. The radical cations of the metallated porphyrins are quite stable and have been easily identified by optical absorption and EPR spectra [22,23]; also, it has been reported that some porphyrins can form π-complexes with its radical cations producing a dimeric radical cation, where the unpaired electron is delocalized over both porphyrin rings [24]. On the other hand, the radical cations of free-base porphyrins are normally transient species, which can only be trapped in frozen glasses [25]. It has been shown that the chemical fate of the initially electrogenerated radical cation of free-base porphyrins is dictated by both the reaction media and the nature of the porphyrin macrocycle, whether it has bulky substituents at the *meso*-positions or not [26]. It has been reported that in solvents which can react with the oxidized forms of the porphyrin, *i.e.* benzonitrile and dichloromethane, the overall products of the oxidation are the monoprotonated (H_3P^+) or diprotonated (H_4P^{2+}) forms of the free-base. Also, it has been suggested that the initial formation of the radical cation of the porphyrin ($H_2P^{\bullet+}$), reaction (1), is followed by a reduction + protonation chemical step to form the monoprotonated porphyrin (H_3P^+); in a step that necessarily involves the reaction with an oxidizable and protic substrate (SH), *i.e.* solvent, reaction (2). It has been stated that for non-hindered prophyrins, the monoprotonated form is stable, so a one-electron oxidation process is observed. For hindered porphyrins, such as tetraphenylporphyrin (H_2TPP), the monoprotonated porphyrin is not stable, and a disproportionation reaction occurs producing both the diprotonated and starting free-base porphyrins, reaction (3), and consequently a two-electron process is observed. *In situ* UV–vis spectroelectrochemical studies have confirmed the formation of these protonated species [26].

$$H_2P \rightleftharpoons H_2P^{\bullet+} + e^- \quad (1)$$

$$H_2P^{\bullet+} + S - H \rightleftharpoons H_3P^+ + S^{\bullet} \quad (2)$$

$$2H_3P^+ \rightleftharpoons H_4P^{2+} + H_2P \quad (3)$$

In the present work, we carried out a comprehensive study by cyclic voltammetry, controlled potential coulometry and *in situ* UV–vis spectroelectrochemistry of four pyrene dendronized porphyrins (Scheme 1) focusing on the protonation reactions of the radical cation of the porphyrin ring in two solvents, CH_2Cl_2 and THF. We show that although the UV–vis spectral changes for the

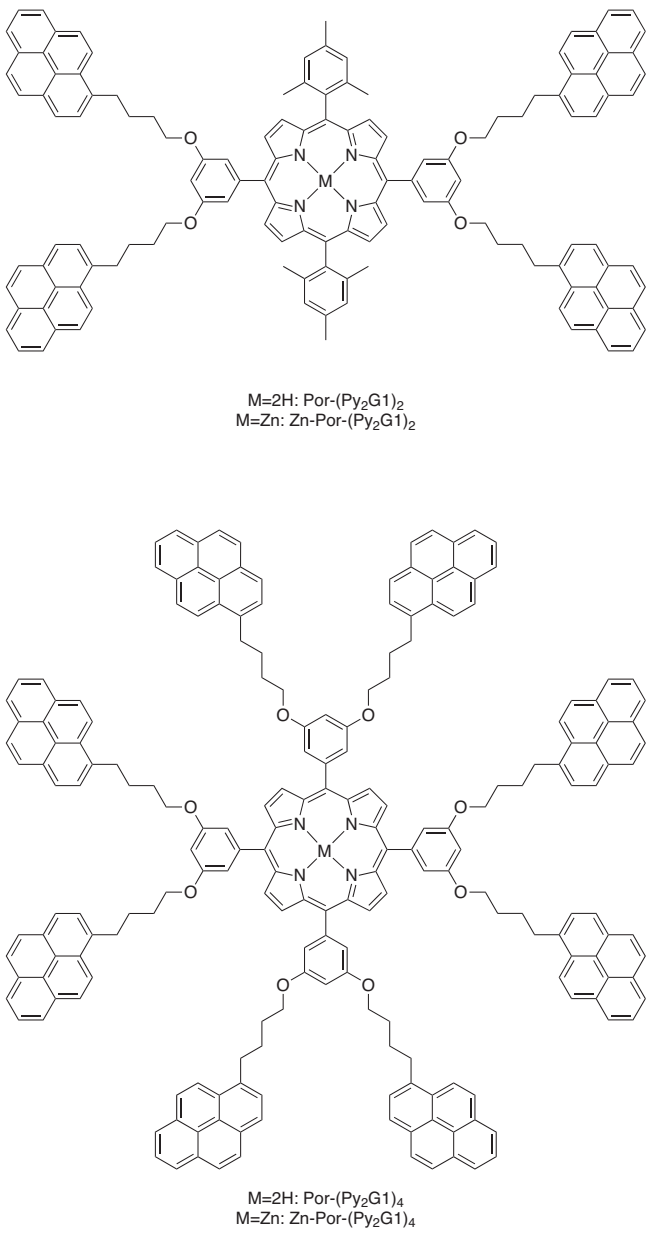

Scheme 1. Chemical structures of the pyrene dendronized porphyrins.

two free-base dendritic molecules, Por-$(Py_2G1)_2$ and Por-$(Py_2G1)_4$, are indicative of the formation of protonated porphyrins, voltammograms of its electrolyzed solutions match those of protonated porphyrins, obtained separately by addition of protic acid, only when the solvent is THF. In the CH_2Cl_2 medium, we demonstrate that the product of the electrolysis corresponds to a paramagnetic species; and that the spectral changes observed during the spectroelectrochemical experiments can be attributed to irradiation itself. Both Zn-Por-$(Py_2G1)_2$ and Zn-Por-$(Py_2G1)_4$, form stable porphyrin radical cations in CH_2Cl_2 and THF.

2. Experimental

2.1. Chemicals and Reagents

The synthesis of the four pyrene dendronized porphyrins (Scheme 1) was carried out according to the method previously reported by us [12]. Anhydrous dichloromethane (CH_2Cl_2, 99.8%, $< 0.001\%$ H_2O), tetrahydrofurane (THF, $\geq 99.5\%$, spectrophotometric grade), and perchloric acid ($HClO_4$, 69 – 72%), obtained

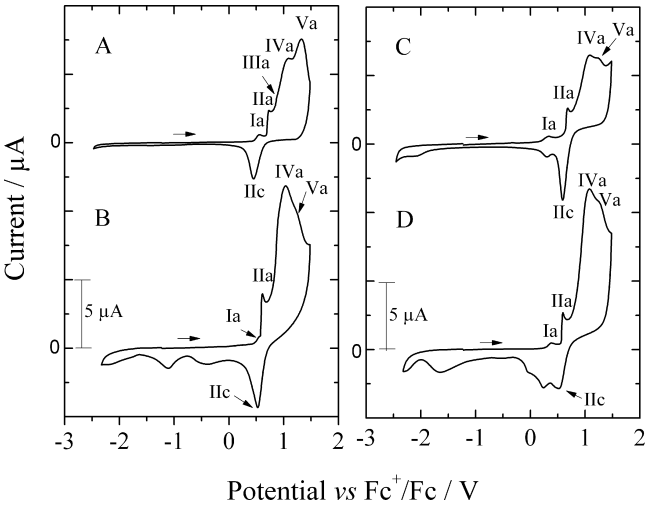

Fig. 1. Experimental voltammograms for 0.5 mM: A) Por-$(Py_2G1)_2$, B) Por-$(Py_2G1)_4$, C) Zn-Por-$(Py_2G1)_2$ and D) Zn-Por-$(Py_2G1)_4$ in 0.1 M Bu_4NPF_6/CH_2Cl_2. Scan rate: 0.1 V/s at 10 °C.

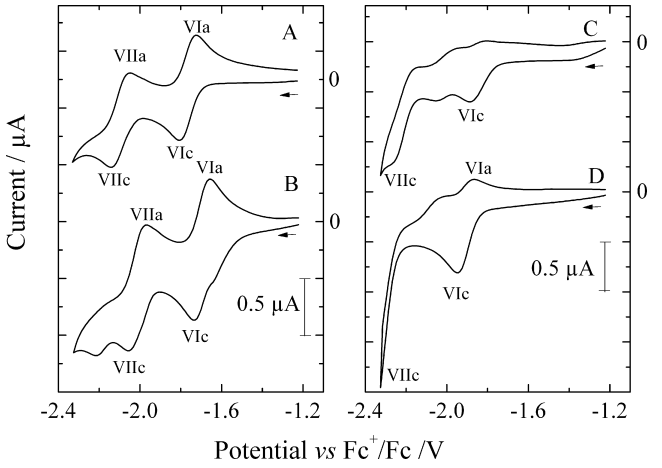

Fig. 2. Experimental voltammograms for 0.5 mM: A) Por-$(Py_2G1)_2$, B) Por-$(Py_2G1)_4$, C) Zn-Por-$(Py_2G1)_2$ and D) Zn-Por-$(Py_2G1)_4$ in 0.1 M Bu_4NPF_6/CH_2Cl_2. Scan rate: 0.1 V/s at 10 °C.

from Sigma-Aldrich, were used as received. Electrochemical grade tetrabutylammonium perchlorate (Bu_4NClO_4, ≥ 99.0%) and tetrabutylammonium hexafluorophosphate (Bu_4NPF_6, ≥ 99.0%) were purchased from Fluka and dried at 60 °C under vacuum prior to use.

2.2. Electrochemical Cells, Electrodes, and Instrumentation

Cyclic voltammetry experiments were carried out in a conventional three-electrode jacketed cell. The working electrode was a 0.3 cm diameter glassy carbon electrode whose effective area was determined to be 0.09 cm^2. The reference electrode was an $Ag/AgNO_3$ electrode (a silver wire immersed in 0.10 M Bu_4NPF_6/0.01 M silver nitrate/acetonitrile). The reference electrode was separated from the test solution by a porous Vycor frit from Bioanalytical Systems. The potential of the reference electrode was periodically measured with respect to the reversible ferrocenium/ferrocene couple, and was found to be 222 ± 5 mV in Bu_4NPF_6 0.1 M/CH_2Cl_2 and 187 ± 3 mV in Bu_4NClO_4 0.1 M/THF. All potentials reported in this work are referred to the Fc^+/Fc couple. Temperature of the jacketed cell was controlled with a circulating bath. The reference electrode was at room temperature (nonisothermal operation). The working electrode was polished with 0.05 μm alumina paste (Buehler), rinsed with water, sonicated for 5 min in distilled water and dried with a tissue. Solutions were purged with ultra high purity nitrogen (Praxair), which was saturated with the solvent before reaching the cell. Voltammograms were recorded in Bu_4NPF_6 0.1 M/CH_2Cl_2 at 0.1 V/s and 10 °C, and −10 °C for the simulations.

Digital simulations were performed using DigiElch 4F, a software for digital simulation of common electrochemical experiments (http://www.digielch.de) [27]. When matching simulations to the experimental voltammograms, the objective was to find the single set of parameter values that provided the best average fit between simulation and experiment for the entire range of concentrations and scan rates employed. This means that a simulation at a given scan rate might be improved by some variation of one or more parameter values, but this could lower the average goodness-of-fit for the entire set of voltammograms. The total uncompensated resistance in Bu_4NPF_6 0.1 M/CH_2Cl_2 at −10 °C (R_u = 3400 Ω) was determined as previously described [28]. Part or none of the solution resistance was compensated electronically and the remainder was included in the simulations.

Controlled potential coulometry was carried out in a 10 mL three-electrode jacketed electrolytic cell. A platinum gauze was used as working electrode, the counter electrode was a platinum wire and $Ag/AgNO_3$ as the reference electrode. A sintered glass disk was used to separate the working and counter electrode compartments. Coulometry was carried out at 10 °C in both Bu_4NPF_6 0.1 M/CH_2Cl_2 and Bu_4NClO_4 0.1 M/THF.

An Autolab PGSTAT 302 potentiostat-galvanostat was used for the cyclic voltammetry and controlled potential electrolysis experiments.

Spectroelectrochemical measurements were conducted using a thin-layer quartz electrochemical cell (path length: 1 mm, BASi) with a three-electrode arrangement, which was coupled to a BASi Epsilon potentionstat-galvanostat. The spectra were obtained using an Agilent 8453 UV–vis spectrophotometer. Working electrode consisted of an optically transparent platinum minigrid, as counter electrode a Pt wire, and $Ag/AgNO_3$ as reference electrode. Working and counter electrodes were separated by a sheet of tracing paper to prevent the diffusion of undesirable chemical species from the counter electrode. The experiments

Table 1
Peak potential and half-peak potential values (V) for the different compounds studied in this work.

Compound	$E_{1/2}$ (**I**)	E_p (**IIa**)	$E_{1/2}$ (**III**)	E_p (**IVa**)	E_p (**Va**)	$E_{1/2}$ (**VI**)	$E_{1/2}$ (**VII**)
H_2TPP	0.52	--	0.85	--	--	-1.69	-2.01
Por-$(Py_2G1)_2$	0.51	0.72	0.85 [a]	1.08	1.27	-1.76	-2.09
Por-$(Py_2G1)_4$	0.56[a]	0.61	0.85	1.03	1.32	-1.70	-2.01
ZnTPP	0.35	--	0.65 [a]	--	--	-1.83	-2.26[c]
Zn-Por-$(Py_2G1)_2$	0.34	0.68	--	1.08	1.26	-1.92[b]	-2.26[c]
Zn-Por-$(Py_2G1)_4$	0.34	0.59	--	1.07	1.27	-1.86 [b]	-2.26[c]

[a] This peak appears overlapped with other signals, the reported value corresponds to the anodic peak potential.
[b] When the potential was switched back after peak VIc a small associated anodic peak was observed
[c] The second reduction process is irreversible, the value corresponds to the anodic peak potential.

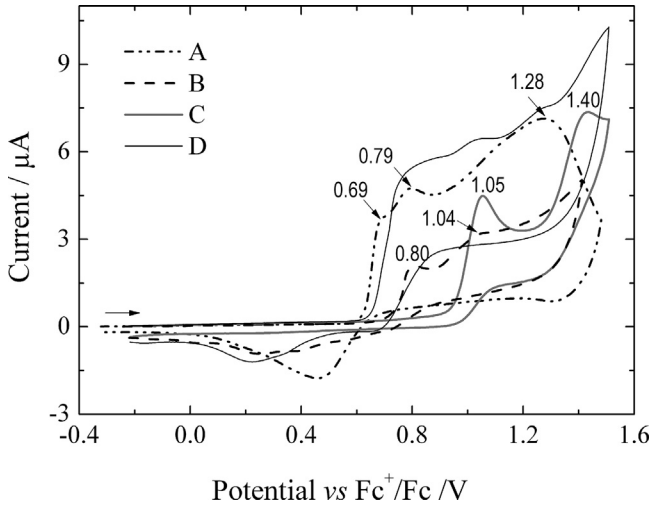

Fig. 3. Experimental voltammograms of 1 mM: A) Py_2G1OH, B) 1-pyrenebutanol, C) 3,5-bis(dodecyloxy)benzyl alcohol, D) 1-pyrenebutanol +0.75 eq 3,5-bis(dodecyloxy)benzyl alcohol in 0.1 M Bu_4NPF_6/CH_2Cl_2. Scan rate: 0.1 V/s at 10 °C.

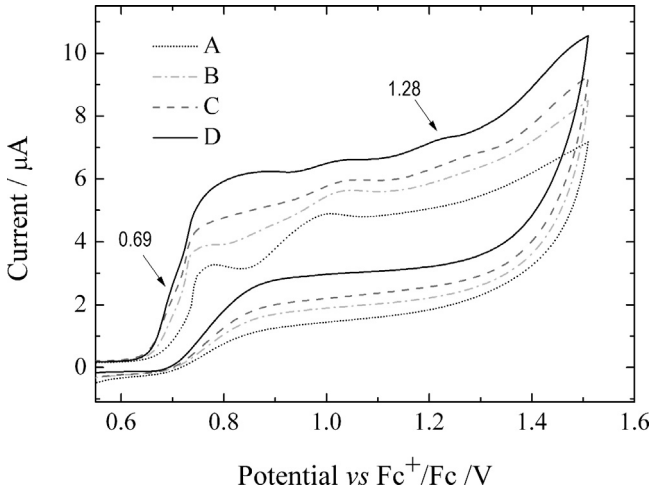

Fig. 4. Experimental voltammograms of 1 mM A) 1-pyrenebutanol, B) +0.25, C) +0.5 and D) +1.0 equivalents of 3,5-bis(dodecyloxy)benzyl alcohol in 0.1 M Bu_4NPF_6/CH_2Cl_2 at 0.1 V/s at 10 °C.

were carried out at room temperature in Bu_4NPF_6 0.1 M/CH_2Cl_2, and Bu_4NClO_4 0.1 M/THF; solutions were deoxygenated with ultra high purity nitrogen (Praxair), which was saturated with the corresponding solvent.

Electron paramagnetic resonance (EPR) spectroscopy experiments were performed at room temperature on a Bruker EPR spectrometer model Elexsys E500. Spectra were recorded in a flat quartz cell either in CH_2Cl_2 or THF at a microwave frequency of 9.778 GHz, 100 kHz field modulation.

3. Results and Discussion

3.1. Voltammetric Analysis

The electrochemical behaviour of four pyrene dendronized porphyrins (Scheme 1) was initially investigated by cyclic voltammetry in Bu_4NPF_6 0.1 M/CH_2Cl_2 (Fig. 1). Voltammograms of Por-$(Py_2G1)_2$ and Por-$(Py_2G1)_4$ show, during the initial positive-going sweep, five oxidation processes, peaks **Ia**-**Va**, with peak **IIIa** barely observed as a small shoulder on peak **IVa**. For Por-$(Py_2G1)_4$, the small peak **Ia** is partially overlapped with peak **IIa** (Fig. 1, curve B). On the reverse scan, a broad cathodic peak **IIc** appears in both compounds, and in the voltammogram of Por-$(Py_2G1)_4$, two additional cathodic peaks are also observed (Fig. 1, curve B). The cathodic peak **IIc** was also seen in voltammograms where the potential was switched back after peak **IIa**, and it was noted that grows in height and shifts to less anodic potentials as the switching potential is extended beyond peak **Va**. In addition, voltammograms encompassing only peak **Ia** showed on the reverse scan a cathodic peak **Ic**, attesting to the reversibility of the electrochemical reaction at peak **Ia**. Zn-Por-$(Py_2G1)_2$ and Zn-Por-$(Py_2G1)_4$ exhibit, on the anodic sweep, a similar behaviour to their equivalent non-metallated compounds, except that the shoulder **IIIa** is buried (Fig. 1, curves C and D).

A study recording the voltammograms towards negative direction revealed that the two free base dendritic porphyrins, Por-$(Py_2G1)_2$ and Por-$(Py_2G1)_4$, present a pair of reversible couples, **VIc**/**VIa** and **VIIc**/**VIIa** (Fig. 2, curves A and B). Voltammograms of the Zn metalated compounds (Fig. 2, curves C and D), also show two main reduction processes, peaks **VIc** and **VIIc**, however, these processes are mostly irreversible. The electrode potential values obtained from the voltammograms of Figs. 1 and 2 are listed in Table 1.

In an effort to assign the process responsible of each peak, we studied the electrochemical behaviour of five reference compounds: tetraphenylporphyrin (H_2TPP) and its metallated form (ZnTPP), to represent the nuclei of the dendritic porphyrin; and the arylalkyl ether dendron of first generation containing two pyrene terminal groups (Py_2G_1OH), 1-pyrenebutanol, and 3,5-bis(dodecyloxy) benzyl alcohol (Scheme 2), representing the branches of the dendritic molecules.

Voltammograms of H_2TPP and ZnTPP present the typical behaviour of porphyrins [20,21,29]. In the oxidative scan, two one-electron reversible peaks corresponding to the formation of porphyrin radical cation and porphyrin dication are observed. On the cathodic scan, two main redox couples leading to porphyrin radical anion and porphyrin dianion are seen. For H_2TPP the two reduction processes are reversible, however, for ZnTPP the second one appears as an irreversible process.

A similar behaviour has been previously reported for other Zn porphyrins [30]. The half wave potential values for these processes are also reported in Table 1. Comparing the peak potential values of H_2TPP and ZnTPP with those of the pyrene dendronized porphyrins (Table 1), peak **Ia** and shoulder **IIIa** can be assigned to the stepwise oxidation of the porphyrin ring. As shown in Fig. 1, in some cases the second oxidation of the porphyrin (**IIIa**) is hidden by peaks **IIa** and **IVa**, which are related to other oxidation processes (*vide infra*).

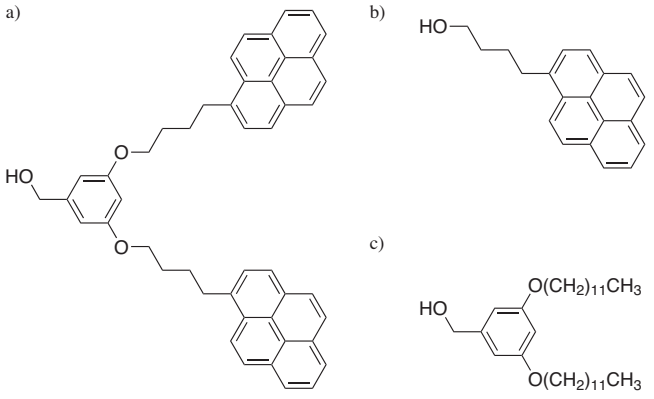

Scheme 2. Chemical structures of the: a) arylalkyl ether dendron of first generation (Py_2G1OH), b) 1-pyrenebutanol and c) 3,5-bis(dodecyloxy)benzyl alcohol.

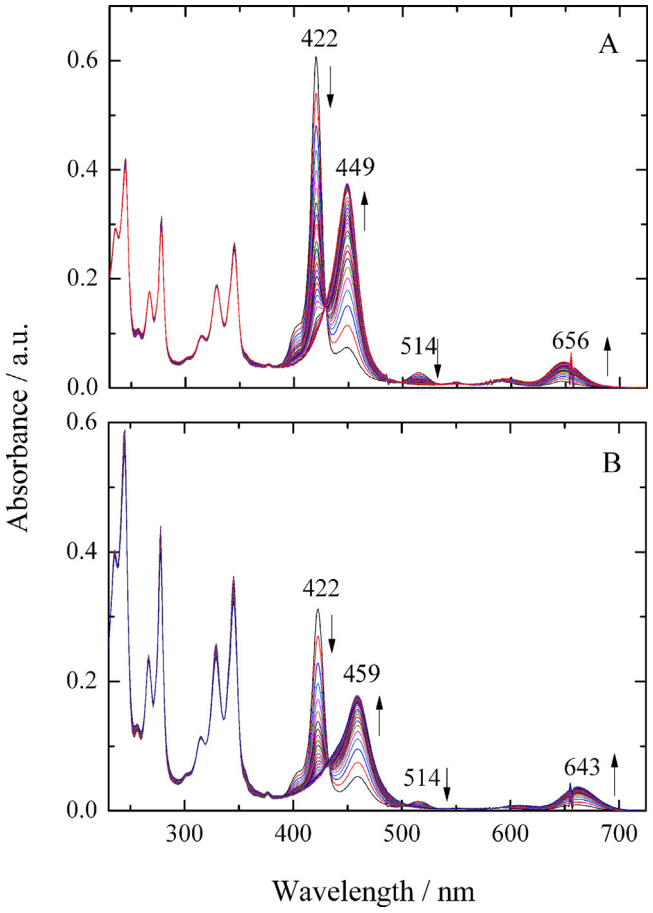

Fig. 5. UV-visible spectral changes in 0.1 M Bu_4NPF_6/CH_2Cl_2 during controlled potential oxidation, in a quartz thin-layer electrochemical cell, for: A) Por-$(Py_2G1)_2$ and B) Por-$(Py_2G1)_4$. No additional bands are observed in the region between 700 and 1000 nm.

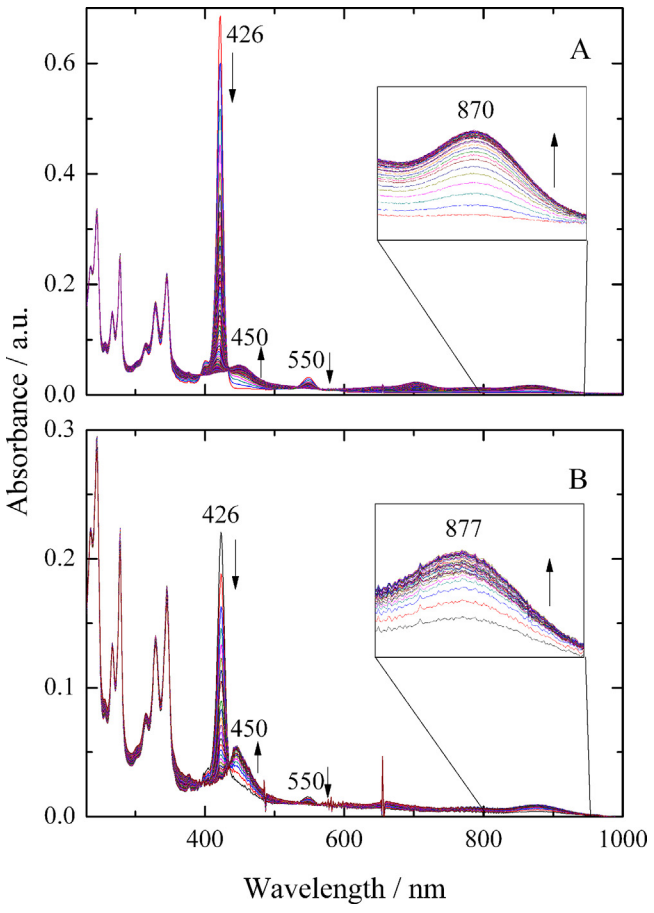

Fig. 6. UV-visible spectral changes in 0.1 M Bu_4NPF_6/CH_2Cl_2 during controlled potential oxidation, in a quartz thin-layer electrochemical cell, for: A) Zn-Por-$(Py_2G1)_2$ and B) Zn-Por-$(Py_2G1)_4$.

On the cathodic sweep, the behaviour of H_2TPP and ZnTPP matches that of their corresponding free-base or metallated pyrene dendronized porphyrins, consequently, the two main reduction processes can be associated with the two consecutive one-electron transfer reactions leading to the radical anion and the dianion of the porphyrin ring.

Cyclic voltammograms of Py_2G_1OH show the presence of three irreversible anodic peaks at 0.69, 0.79 and 1.28 V (Fig. 3, curve A). In order to distinguish the oxidation processes centered on the pyrene moiety from those on the arylalkyl ether unit, voltammograms of 1-pyrenebutanol and 3,5-bis(dodecyloxy) benzyl alcohol were also recorded. It was found that both molecules are oxidized through two irreversible anodic steps, with peak potentials at 0.80 and 1.04 V for the pyrene moiety (Fig. 3, curve B), and 1.05 and 1.40 V for the arylalkyl ether moiety (Fig. 3, curve C). This study revealed that the voltammogram of Py_2G_1OH does not simply correspond to the sum of the oxidation peaks of pyrene and arylalkyl ether electroactive moieties. The fact that the peaks at 0.69 and 1.28 V in the voltammogram of Py_2G_1OH are not present for 1-pyrenebutanol or 3,5-bis(dodecyloxy) benzyl alcohol, suggests some kind of interaction between both electroactive units. This assumption was further supported by the fact that when 3,5-bis(dodecyloxy) benzyl alcohol was added to a solution of 1-pyrenebutanol, a faintly perceptible shoulder at about 0.69 and a small peak at 1.28 V appeared (Fig. 3, curve D), and becomes evident as the concentration of benzyl alcohol increases (Fig. 4). From these voltamperometric studies it is possible to state that the oxidation peak **IIIa** is related not only to the second oxidation of the porphyrin ring, but also to the first oxidation process of the pyrene moieties, which are oxidized at around 0.80 V. As seen from Table 1, peak **IIa** observed at the CV of the pyrene dendronized porphyrins corresponds to that observed at 0.69 V in the voltammogram of the dendron (Py_2G_1OH), although for those compounds containing eight pyrene terminal groups, peak **IIa** is shifted by about 0.10 V to less anodic values. Finally, the broad peak **IVa**, along with peak **Va,** are linked to the second oxidation process of pyrene and the two oxidation processes of the arylalkyl ether units.

3.2. Spectroelectrochemical Measurements in CH_2Cl_2.

Afterwards, we focused our attention on studying the formation and evolution of the porphyrin radical cation species in the dendritic molecules. For this purpose, *in situ* UV–vis spectroelectrochemical experiments were conducted using a quartz thin-layer electrochemical cell coupled to a UV-visible spectrophotometer. Controlled potential electrooxidation was carried out at ~0.15 V after the potential of peak **Ia**, and the products were monitored by recording absorption spectra every two seconds during 120 seconds. Fig. 5 shows the results obtained for the two free-base dendrimers, Por-$(Py_2G1)_2$ and Por-$(Py_2G1)_4$. It can be noted that as the oxidation proceeds, the Soret band (422 nm) decreases and, simultaneously, a new Soret-like band appears and increases over time (449 nm for Por-$(Py_2G1)_2$ and 459 nm for Por-$(Py_2G1)_4$); also, there is a decrease of the Q-IV band at 514 nm and an increase of the Q-I band at around 643–656 nm. As expected, the bands in the region of 230 to 350 nm, corresponding to the pyrene groups, are not modified during the electrooxidation at peak **Ia**. Since the reference compound, H_2TPP, showed the same spectral changes (*vide infra*) than the two free-base

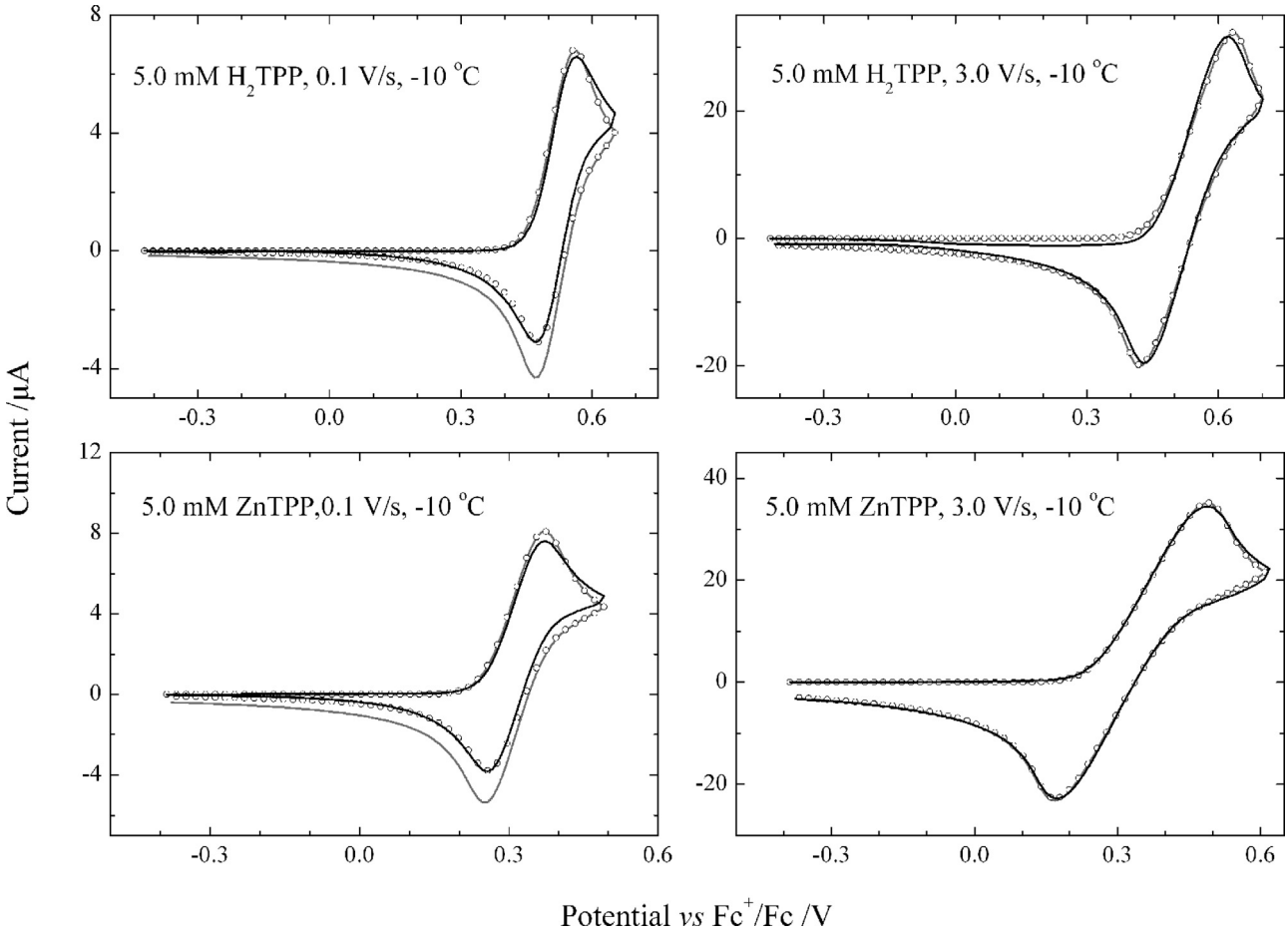

Fig. 7. Background-corrected cyclic voltammograms of 5.0 mM H_2TPP (top row) and ZnTPP (bottom row) in CH_2Cl_2 with 0.10 M Bu_4NPF_6 (black). Simulation based on the one-electron oxidation from neutral to radical cation (gray). Simulation including a decomposition reaction of the radical cation to form some unknown product (symbols), with simulation parameter values as listed in Table 2.

dendritic porphyrins, it can be stated that the Py_2G1 dendrons attached to the *meso*-positions of the porphyrin macrocycle do not alter the electrochemical behaviour of the first electrooxidation process of the porphyrin ring. A spectral pattern similar to that shown in Fig. 5 has also been reported during the electro-oxidation of H_2TPP in benzonitrile [26] and for some phosphorylated free-base porphyrins in CH_2Cl_2 [31]. Because these spectral features match those reported for the stepwise acidification of neutral porphyrins [25,32,33], the final product of the electrooxidation of porphyrins has been usually assigned to doubly protonated porphyrins. The formation of these species has been explained by Le Mest et al. through the sequence of reactions (1) to (3) [26].

The UV–vis spectral changes accompanying the one-electron oxidation of the metallated dendrimers are quite different from those of their free-base analogues (Fig. 6). As the potential is kept at that corresponding to peak **Ia**, the intensity of the Soret (426 nm) and Q (550 nm) bands decreases; also a band at 870–877 nm appears and grows in intensity as the oxidation proceeds. The decrease in the intensity of the Soret band is typical of an oxidation process centered at the conjugated π-system of the porphyrin ring [31]; and the presence of the band at around 870–877 nm has been assigned to the absorption of the radical cation of the porphyrin [34]. Analogous spectral changes were observed during the oxidation of the reference compound ZnTPP.

Table 2
Simulation parameters used in the simulation of voltammograms of H_2TPP and ZnTPP in Bu_4NPF_6 0.1 M/CH_2Cl_2, -10 °C.

		(M)TPP ⇄ (M)TPP$^{\bullet+}$ + e		(M)TPP$^{\bullet+}$ → Prod		
Compound	Conc./mmol dm^{-3}	E^0_1/V	k^0_1/cm s^{-1}	K	k_f/s^{-1}	D/cm^{2}s^{-1}
H_2TPP	2.52	0.729	0.035	1×10^7	0.29	4.9×10^{-6}
H_2TPP	5.05	0.725	0.035	1×10^7	0.28	4.7×10^{-6}
ZnTPP	2.48	0.492	0.025	1×10^7	0.14	5.1×10^{-6}
ZnTPP	4.97	0.495	0.025	1×10^7	0.15	4.9×10^{-6}

The same values were used to fit all scan rates from 0.1 to 3.0 V/s. Potentials are referred to the formal potential of the ferrocenium/ferrocene couple. The electron-transfer coefficient, α, was set equal to 0.50 for all electrode reactions. The solution resistance was partially compensated via IR compensation through positive feedback (680 Ω) and the remaining resistance (2400 Ω) was incorporated in the simulations.

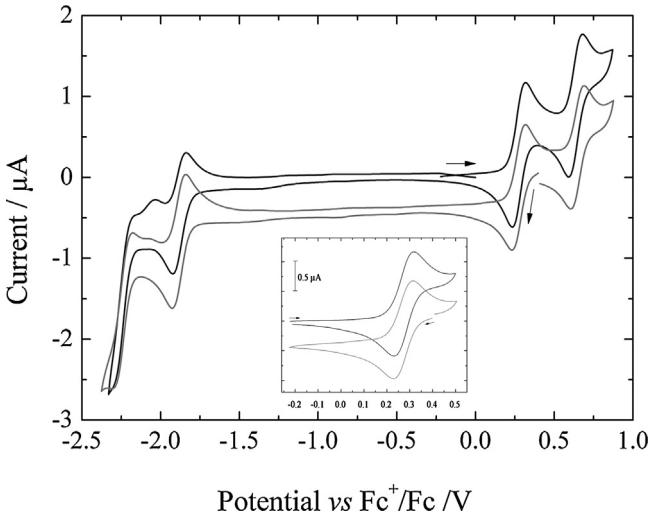

Fig. 8. Voltammograms of 0.5 mM ZnTPP before (black line) and after (gray line) electrolysis in CH_2Cl_2 containing 0.1 M Bu_4NPF_6. Scan rate: 0.1 V/s at 10 °C. Insert: Voltammograms encompassing only the first oxidation wave.

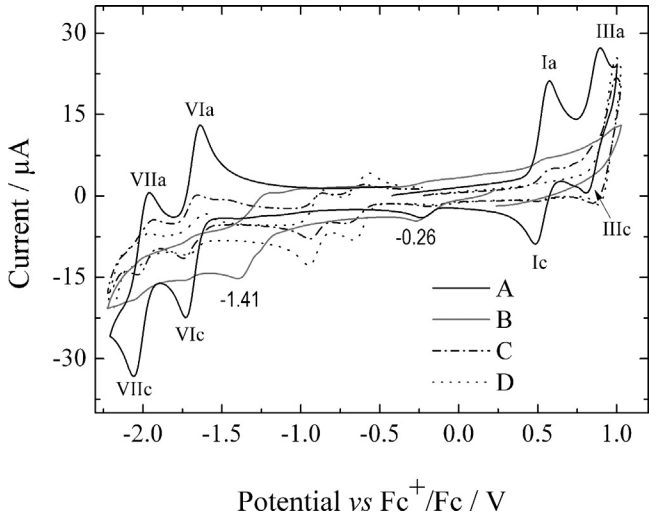

Fig. 9. Voltammograms of 0.5 mM H_2TPP before (A) and after (B) electrolysis; and H_2TPP in the presence of one (C) and two (D) equivalents of $HClO_4$ in CH_2Cl_2 containing 0.1 M Bu_4NPF_6. Scan rate: 0.1 V/s at 10 °C.

3.3. Electrochemical Measurements of H_2TPP and ZnTPP.

Based on the fact that the spectroelectrochemical experiments for both H_2TPP and ZnTPP presented essentially the same behaviour than their corresponding free-base and metallated pyrene dendronized porphyrins, in the following experiments these model molecules were used as reference compounds to carry out a deeper electrochemical study of the processes taking place at the first oxidation peak of the porphyrin system.

As mentioned above, ZnTPP and H_2TPP are reversibly oxidized to the corresponding radical cation at the first anodic wave. A careful analysis by digital simulation of the voltammograms encompassing only the first wave evidenced a small loss of reversibility, which was more evident for scan rates lower than 0.3 V/s. In order to account for these results, a first-order loss of the radical cation, which was treated as a totally irreversible reaction (large equilibrium constant) had to be included in the simulations, with k_f values of 0.28 and 0.15 s^{-1} at −10 °C, for H_2TPP and ZnTPP, respectively. Introduction of other reactions into the simulation, such as the bimolecular dimerization of the radical cation, could not account for the experimental data. These results show that in the timescale of the cyclic voltammetry, the radical cation is fairly stable for both compounds. Simulations were carried out for voltammograms recorded at scan rates from 0.10 to 3.00 V/s and for two different concentrations of porphyrin. The simulation parameter values that provided the best fit for all rates and concentrations are presented in Table 2. Examples of the fits to the experimental voltammograms are also shown in Fig. 7.

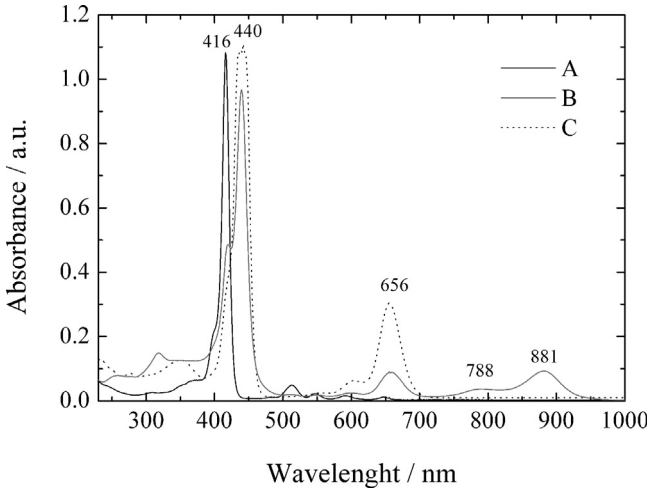

Fig. 10. Absorption spectra of H_2TPP in CH_2Cl_2: A) before and B) after electrolysis; and C) in the presence of two equivalents of $HClO_4$.

Exhaustive controlled potential coulometry was carried out at the first anodic peak for 0.5 mM of H_2TPP and ZnTPP in 0.1 M Bu_4NPF_6/CH_2Cl_2. It was found that the electrolysis was essentially complete after about 20 min, where the charge no longer changed with time. Through application of Faraday's law, the n-values measured corresponded to one-electron per molecule for both compounds. Fig. 8 presents cyclic voltammograms recorded for a solution of ZnTPP before and after the electrolysis. The insert shows that the oxidation peak has disappeared and is replaced by the reduction peak encountered on an initial scan in the negative direction, suggesting the formation of the radical cation. Reduction of the solution of the radical cation formed during the electrolysis recovered 80% of the charge for ZnTPP, which is in agreement with the small irreversible decomposition of the radical cation found by simulation at −10 °C. Additionally, the absence of new peaks in the full scan indicates that, under these conditions, no following chemical reactions of the radical cation occur. These findings suggest that only a tiny amount of an electrochemically inert decomposition product is formed. UV-vis and EPR spectra of the electrolyzed solution also confirm the presence of the paramagnetic $ZnTPP^{\bullet+}$.

Unlike ZnTPP, for H_2TPP no evidence of a stable radical cation could be found. Voltammograms of its electrolyzed solutions show that the two oxidation couples vanished, whilst two new irreversible reduction peaks at −0.26 and −1.41 V appeared (Fig. 9, curve B). Reductive electrolysis of the electrolyzed solution at the potential of these new waves did not regenerate the original voltammogram, attesting to the irreversibility of the oxidation process. On the other hand, the fact that we obtained n = 1 in exhaustive coulometry implies that the mechanism involving formation of diprotonated species is not feasible. But, since the spectroelectrochemical experiments clearly suggest the formation of the protonated species, we then focused our attention on trying to get evidences of their presence by other means. For this purpose, cyclic voltammograms of a freshly prepared solution of H_2TPP in presence of one and two equivalents of $HClO_4$ were recorded and compared with the voltammogram of the electrolyzed solution

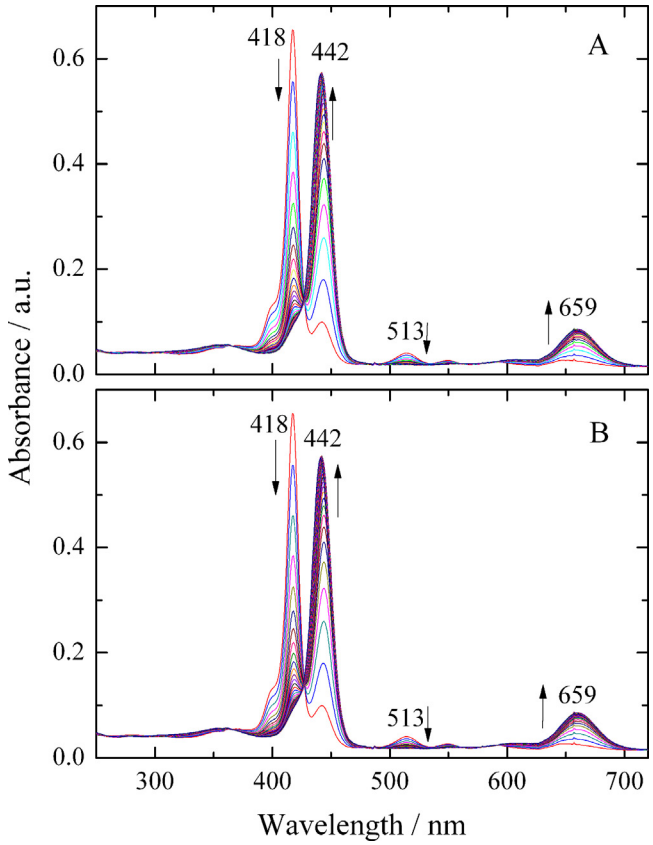

Fig. 11. UV-visible spectral changes for H_2TPP in 0.1 M Bu_4NPF_6/CH_2Cl_2in aquartz thin-layer electrochemical cell: A) during a controlled potential oxidation at peak Ia, and B) without a potential applied. No additional bands are observed in the region between 700 and 1000 nm.

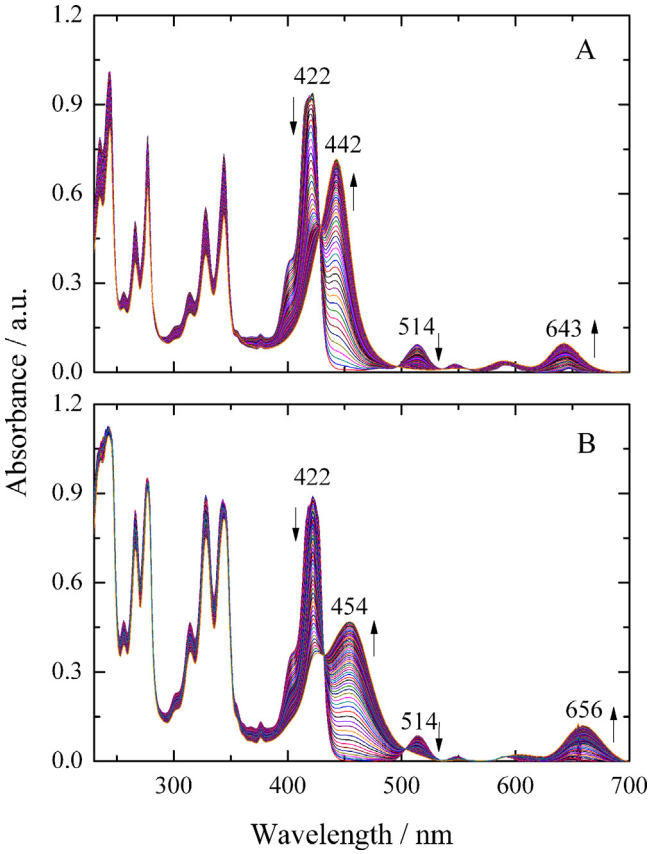

Fig. 12. UV-visible spectral changes in 0.1 M Bu_4NPF_6/CH_2Cl_2 during controlled potential oxidation, in a quartz thin-layer electrochemical cell, for: A) Por-$(Py_2G1)_2$ and B) Por-$(Py_2G1)_4$. No additional bands are observed in the region between 700 and 1000 nm.

(Fig. 9). The lack of correspondence between the observed peaks confirms that the porphyrin protonated species are not the final product from the electrooxidation of H_2TPP in CH_2Cl_2. Even though both the electrolyzed solution and the one with $HClO_4$ were green, the shade was clearly different. Additionally, it was proved that the absorption spectra of a solution of H_2TPP in presence of one- or two-equivalents of acid show different spectral features than those of the solution of H_2TPP after exhaustive electrolysis (Fig. 10). This figure shows that although both spectra present a red shift of the Soret band of nearly 24 nm, and an enhancement of the intensity of the Q-IV band (656 nm), the spectrum of the electrolyzed solution contains two bands at 788 and 881 nm that are not present in the $H_2TPP + H^+$ spectra. Besides, the EPR spectrum of the electrooxidized porphyrin produced a signal at $g = 2.002$ with $\Delta B_{p-p} = 6.76$ G, while the solution of the protonated porphyrin did not show any signal. It is important to mention that although the paramagnetic species formed by exhaustive controlled potential coulometry seems to be quite stable in solution, as shown by the fact that the EPR spectrum was recorded about 40 min after electrolysis, all our attempts to separate the green product from the electrolyte were futile. During the workup, the initially obtained green product turned brown, and the formation of other products was evident by the presence of new spots on thin-layer chromatography.

The spectroelectrochemical and the controlled potential electrolysis results indicate that the porphyrin oxidation product is different in each case. To rule out any influence from the irradiation on the chemical reactivity of the radical cation, experiments using the spectroelectrochemical cell were carried out for a solution of H_2TPP in CH_2Cl_2 without applying an oxidation potential (Fig. 11B). From this figure, it is evident that the irradiation of the solution at wavelengths between 200 and 1000 nm yielded the same spectral changes as the spectroelectrochemical experiment at controlled potential oxidation (~0.15 V after peak **Ia**) (Fig. 11A). In contrast with the product obtained from the exhaustive coulometry, the irradiated H_2TPP solution does not show the presence of a paramagnetic species. These findings suggest that, for the free-base porphyrins in CH_2Cl_2, photoexcitation itself leads to the diprotonated species, H_4TPP^{2+}, as it has been previously reported for the irradiation of H_2TPP in $CHCl_3$ solutions at wavelengths between 289 and 337 nm [25]. It is important to mention that irradiation of metallated porphyrins (ZnTPP, Zn-Por-$(Py_2G1)_2$, and Zn-Por-$(Py_2G1)_4$) in CH_2Cl_2 did not produce any spectral changes.

3.4. Electrochemical and Spectroelectrochemical Measurements in THF.

Due to the reactive nature of the chlorocarbon solvents under the experimental conditions, we decided to use THF, which proved to be a better solvent choice for the *in situ* UV–vis spectroelectrochemical experiments since all the dendritic molecules were soluble, and the irradiation of these compounds in THF solution did not produce any chemical or spectral change. The evolution of the UV–vis spectra obtained during controlled potential oxidation of the free-base Por-$(Py_2G1)_2$ and Por-$(Py_2G1)_4$ in THF solution is illustrated in Fig. 12. As it can be seen, the spectral changes again match those reported for the formation of protonated species [26,31], but now with the certainty that these changes are strictly produced by the electrooxidation process.

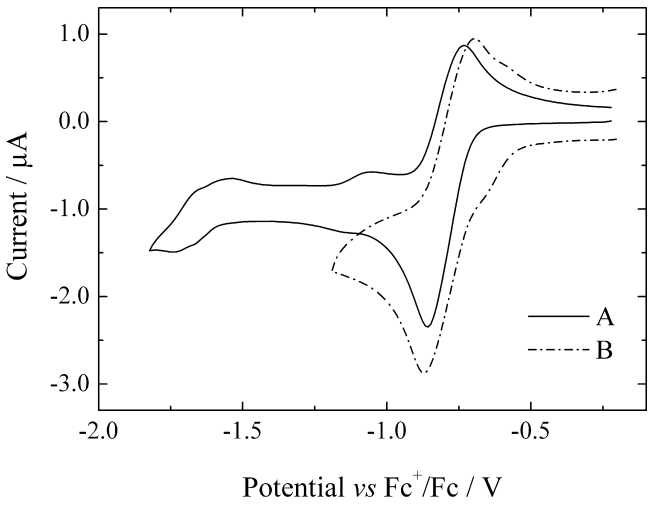

Fig. 13. Voltammograms of 0.5 mM H_2TPP after electrolysis (A) and in presence of two equivalents of $HClO_4$ (B) in THF containing 0.1 M Bu_4NClO_4. Scan rate: 0.1 V/s at 10 °C.

Since H_2TPP showed the same spectroelectrochemical behaviour than the two free-base dendritic porphyrins, we again used it as a model to go deeper on the understanding of the electroxidation mechanism. When a solution of H_2TPP in THF was electrolyzed at the potential of the peak **Ia**, 0.66 V *vs* Fc^+/Fc, it was found that the global process taking place at this first oxidation step involves two-electrons per molecule, and the solution turned from violet to dark green. This behaviour has been already described for the oxidation of H_2TPP in benzonitrile [26] and it has been attributed to the formation of doubly protonated species, following the reactions (1) to (3). Also, the agreement of the voltammograms of the electrolyzed solution with that of a solution of H_2TPP with two-equivalents of $HClO_4$ further supports the fact that the oxidation of free-base porphyrins leads to the formation of the protonated species in this solvent (Fig. 13). Additionally, no signal is observed in EPR spectroscopy. Spectroelectrochemical experiments of the metallated dendrimers, Zn-Por-$(Py_2G1)_2$ and Zn-Por-$(Py_2G1)_4$, in THF showed a similar behaviour to that found in CH_2Cl_2 (Fig. 6), where the spectral changes were indicative of the presence of the porphyrin radical cation. EPR analysis of an electrochemically oxidized solution of ZnTPP in THF confirmed the presence of the phorphyrin radical cation, with an EPR signal at g = 2.001 and ΔB_{p-p} = 6.84 G.

4. Conclusions

A family of four dendritic molecules containing a porphyrin core connected to a first generation Fréchet-type dendron (Py_2G1) with pyrene groups at the periphery was studied by a combination of electrochemical and UV–vis spectroelectrochemical techniques. Cyclic voltammetry experiments show that the three main constitutive units of the dendrimers, pyrene, arylalkyl ether and porphyrin, are electrochemically active. On the positive potential sweep, an anodic peak, corresponding to a process centered on the porphyrin ring, was identified, followed by several irreversible oxidation processes, which were assigned to the pyrene and arylalkyl ether moieties of the dendrimer branches. On the cathodic sweep only the porphyrin ring was electroactive and the two well-known reversible reduction processes, corresponding to the radical anion and dianion, were observed. Since the pyrene groups are connected through saturated bonds to the tetraphenyl porphyrin ring, they do not modify the potential of the porphyrin in a significant way.

Electrochemical and UV–vis spectroelectrochemical experiments show that when the porphyrin bears a coordinated Zn, as in Zn-Por-$(Py_2G1)_2$ and Zn-Por-$(Py_2G1)_4$, the product of the first oxidation process is the porphyrin radical cation, whose main spectral characteristics are the decrease of the Soret band at 426 nm, and the growth of a new absorption band in the region of 870–877 nm; and the EPR signal at g = 2.001 with a peak to peak separation of 6.84 G. In contrast, for the free-base porphyrins, Por-$(Py_2G1)_2$ and Por-$(Py_2G1)_4$, the reactivity of the radical cation depends on the solvent. In THF, an overall two-electron process was observed for the first oxidation peak, and the formation of H_4TPP^{2+} species was confirmed by cyclic voltammetry. However, in CH_2Cl_2 an overall one-electron process took place, and the product was identified as a paramagnetic species that is stable in solution; both cyclic voltammetry and absorption spectra rule out the formation of either the radical cation or a protonated porphyrin species. These findings differ from what has been previously reported for other porphyrins in CH_2Cl_2 [26,31], where the formation of doubly protonated porphyrin species has been attributed to the electrooxidation. Here we demonstrate that UV–vis light irradiation of the porphyrin solution by itself can account for the observed spectral evolution.

Acknowledgements

We thank to the Consejo Nacional de Ciencia y Tecnología (CONACYT) for the financial support for this research through grants No. P43984-Q and 128788, E.K.G-M and G. Z-G are grateful to CONACYT for their PhD grants and to Programa de Posgrado en Ciencias Químicas, UNAM. We thank Dr. Alejandro Solano-Peralta for his help recording the EPR spectra.

References

[1] G.R. Newkome, Z. Yao, G.R. Baker, V.K. Gupta, Micelles. Part 1. Cascade molecules: a new approach to micelles. A [27]-arborol, J. Org. Chem. 50 (1985) 2003–2004, doi:http://dx.doi.org/10.1021/jo00211a052.
[2] C. Wörner, R. Mülhaupt, Polynitrile- and polyamine-functional poly(trimethylene imine) dendrimers, Angew. Chemie Int. Ed. English. 32 (1993) 1306–1308, doi:http://dx.doi.org/10.1002/anie.199313061.
[3] D.A. Tomalia, Birth of a new macromolecular architecture: dendrimers as quantized building blocks for nanoscale synthetic polymer chemistry, Prog. Polym. Sci. 30 (2005) 294–324, doi:http://dx.doi.org/10.1016/j.progpolymsci.2005.01.007.
[4] A., Nantalaksakul, D., Reddy, C., Bardeen, S., Thayumanavan, Light harvesting dendrimers, Photosynth. Res. ; 87 (2006) 133–158, http://dx.doi.org/10.1007/s11120–005-8387–3>http://dx.doi.org/10.1007/s11120–005-8387–3/<a>
[5] P. Ceroni, M. Venturi, Photoactive and electroactive dendrimers: future trends and applications, Aust. J. Chem. 64 (2011) 131–146, doi:http://dx.doi.org/10.1071/CH10326.
[6] H.D. Abruña, Redox and photoactive dendrimers in solution and on surfaces, Anal. Chem. 76 (2004) 310A–319A, doi:http://dx.doi.org/10.1021/ac041623o.
[7] P. Ceroni, G. Bergamini, F. Marchioni, V. Balzani, Luminescence as a tool to investigate dendrimer properties, Prog. Polym. Sci. 30 (2005) 453–473, doi:http://dx.doi.org/10.1016/j.progpolymsci.2005.01.003.
[8] A. Adronov, J.M.J. Fréchet, Light-harvesting dendrimers, Chem, Commun. 170 (2000) 1701–1710, doi:http://dx.doi.org/10.1039/b005993p.
[9] J.M.J. Fréchet, Dendrimers and other dendritic macromolecules: from building blocks to functional assemblies in nanoscience and nanotechnology, J. Polym. Sci. Part A Polym. Chem. 41 (2003) 3713–3725, doi:http://dx.doi.org/10.1002/pola.10952.
[10] V. Balzani, Light-harvesting dendrimers, Curr. Opin. Chem. Biol. 7 (2003) 657–665, doi:http://dx.doi.org/10.1016/j.cbpa.2003.10.001.
[11] D. Garrot, B. Langlois, C. Roquelet, T. Michel, P. Roussignol, C. Delalande, E. Deleporte, J.-S. Lauert, C. Voisin, Time-resolved investigation of excitation energy transfer in carbon nanotube-porphyrin compounds, J. Phys. Chem. C. 115 (2011) 23283–23292, doi:http://dx.doi.org/10.1021/jp207267e.
[12] G. Zaragoza-Galán, M. Fowler, R. Rein, N. Solladié, J. Duhamel, E. Rivera, Fluorescence resonance energy transfer in partially and fully labeled pyrene dendronized porphyrins studied with model free analysis, J. Phys. Chem. C. 118 (2014) 8280–8294, doi:http://dx.doi.org/10.1021/jp501445n.
[13] T. Umeyama, H. Imahori, Photofunctional hybrid nanocarbon materials, J. Phys. Chem. C. 117 (2013) 3195–3209, doi:http://dx.doi.org/10.1021/jp309149s.

[14] D.M. Guldi, G.M.A. Rahman, N. Jux, D. Balbinot, U. Hartnagel, N. Tagmatarchis, M. Prato, Functional single-wall carbon nanotube nanohybrids-associating SWNTs with water-soluble enzyme model systems, J. Am. Chem. Soc. 127 (2005) 9830–9838, doi:http://dx.doi.org/10.1021/ja050930o.
[15] E. Maligaspe, A.S.D. Sandanayaka, T. Hasobe, O. Ito, F. D'souza, Sensitive efficiency of photoinduced electron transfer to band gaps of semiconductive single-walled carbon nanotubes with supramolecularly attached zinc porphyrin bearing pyrene glues, J. Am. Chem. Soc. 132 (2010) 8158–8164, doi:http://dx.doi.org/10.1021/ja101776p.
[16] Q. Zhong, V.V. Diev, S.T. Roberts, P.D. Antunez, R.L. Brutchey, S.E. Bradforth, M.E. Thompson, Fused porphyrin-single-walled carbon nanotube hybrids: efficient formation and photophysical characterization, ACS Nano 7 (2013) 3466–3475, doi:http://dx.doi.org/10.1021/nn400362e.
[17] F. D'Souza, A.S.D. Sandanayaka, O. Ito, SWNT-based supramolecular nano-architectures with photosensitizing donor and acceptor molecules, PJ. Phys. Chem. Lett. 1 258 (2010) 2586–2593, doi:http://dx.doi.org/10.1021/jz1009407.
[18] J. Bartelmess, B. Ballesteros, G. de la Torre, D. Kiessling, S. Campidelli, M. Prato, T. Torres, D.M. Guldi, Phthalocyanine-pyrene conjugates: a powerful approach toward carbon nanotube solar cells, J. Am. Chem. Soc. 132 (2010) 16202–16211, doi:http://dx.doi.org/10.1021/cr900254z.
[19] D. Gust, T.A. Moore, A.L. Moore, Mimicking photosynthetic solar energy transduction, Acc. Chem. Res. 34 (2001) 40–48, doi:http://dx.doi.org/10.1021/ar9801301.
[20] K.M. Kadish, E. Van Caemelbecke, G. Royal, Electrochemistry of metalloporphyrins in nonaqueous media, in: K.M. Kadish (Ed.), Porphyr. Handb., Academic Press, San Diego, CA, 2000, pp. 1–114.
[21] K.M., Kadish, E., Van, Caemelbecke, G., Royal, The Porphyrin Handbook vol. 8 Electron Transfer, Academic Press USA, 2000
[22] Z. Gasyna, W.R. Browett, M.J. Stillman, One-electron, visible-light photooxidation of porphyrins in alkyl chloride solutions, Inorg. Chem. 23 (1984) 382–384, doi:http://dx.doi.org/10.1021/ic00171a024.
[23] G.L.W. Potter, R.N. Young, Light-induced simultaneous photooxidation and photoreduction of zinc tetraphenylporphyrin radical cation, J. Am. Chem. Soc. Commun. 102 (1980) 2471–2473, doi:http://dx.doi.org/10.1021/ja00527a063.
[24] A. Takai, C.P. Gros, J.-M. Barbe, R. Guilard, S. Fukuzumi, Enhanced electron-transfer properties of cofacial porphyrin dimers through interactions, Chem. - A Eur. J. 15 (2009) 3110–3122, doi:http://dx.doi.org/10.1002/chem.200802166.
[25] Z. Muñoz, A.S. Cohen, L.M. Nguyen, T.A. McIntosh, P.E. Hoggard, Photocatalysis by tetraphenylporphyrin of the decomposition of chloroform, Photochem. Photobiol. Sci. 7 (2008) 337–343, doi:http://dx.doi.org/10.1039/b713270k.
[26] C. Inisan, J.-Y. Saillard, R. Guilard, A. Tabard, Y. Le Mest, Electrooxidation of porphyrin free bases: fate of the -cation radical, New J Chem. 82 (1998) 823–830, doi:http://dx.doi.org/10.1039/A803974G.
[27] M. Rudolph, Digital simulations on unequally spaced grids. Part 2. Using the box method by discretisation on a transformed equally spaced grid, J. Electroanal. Chem. 543 (2003) 23–39, doi:http://dx.doi.org/10.1016/S0022–0728(02) 1,257-3.
[28] N.A. Macías-Ruvalcaba, D.H. Evans, Study of the effects of ion pairing and activity coefficients on the separation in standard potentials for two-step reduction of dinitroaromatics, J. Phys. Chem. B. 109 (2005) 14642–14647, doi:http://dx.doi.org/10.1021/jp051641p.
[29] H. Sun, J.C. Biffinger, S.G. DiMagno, Ion pairing in tetraphenylporphyrin oxidation: a semiquantitative study, Dalt Trans (2005) 3148–3154, doi:http://dx.doi.org/10.1039/b506109a.
[30] Y. Le Mest, M. L'Her, N.H. Hendricks, K. Kim, J.P. Collman, Electrochemical and spectroscopic properties of dimeric cofacial porphyrins with nonelectroactive metal centers. Delocalization processes in the porphyrin cation-radical systems, Inorg. Chem. 31 (1992) 835–847, doi:http://dx.doi.org/10.1021/ic00031a028.
[31] K.M. Kadish, P. Chen, Y.Y. Enakieva, S.E. Nefedov, Y.G. Gorbunova, A.Y. Tsivadze, A. Bessmertnykh-Lemeune, C. Stern, R. Guilard, Electrochemical and spectroscopic studies of poly(diethoxyphosphoryl) porphyrins, J. Electroanal. Chem. 656 (2011) 61–71, doi:http://dx.doi.org/10.1016/j.jelechem.2011.01.011.
[32] G. De Luca, A. Romeo, L.M. Scolaro, Counteranion dependent protonation and aggregation of tetrakis(4-sulfonatophenyl) porphyrin in organic solvents, J. Phys. Chem. B. 110 (2006) 7309–7315, doi:http://dx.doi.org/10.1021/jp0530348.
[33] G.S.S. Saini, O.K. Medhi, A.L. Verma, Simultaneous formation of mono- and dications of free-base tetraphenylporphin during photo-oxidation probed by resonance Raman and absorption techniques, Chem. Phys. Lett. 322 (2000) 293–299, doi:http://dx.doi.org/10.1016/S0009–2614(00) 414–0.
[34] J. Fajer, D.C. Borg, A. Forman, D. Dolphin, R.H. Felton, Cation radicals and dications of metalloporphyrins, J. Am. Chem. Soc. 92 (1970) 3451–3459, doi:http://dx.doi.org/10.1021/ja00714a038.